Proton elastic scattering on light nuclei. II. Nuclear structure effects

E. Fabrici, S. Micheletti, M. Pignanelli, and F. G. Resmini
Istituto di Fisica dell'Università di Milano and Istituto Nazionale di Fisica Nucleare, Sezione di Milano, Milano, Italy

R. De Leo, G. D'Erasmo, and A. Pantaleo
Istituto di Fisica dell'Università di Bari and Istituto Nazionale di Fisica Nucleare, Sezione di Bari, Bari, Italy
(Received 22 June 1979)

Differential cross sections for proton scattering on 61 nuclei with mass numbers between 9 and 70 were measured at 35.2 MeV incident energy. To extend previous measurements further data were collected at 29.7 MeV on 10 nuclei. From a detailed inspection of the data a definite correlation emerges between the elastic and inelastic cross section values at backward angles and the quadrupole deformation parameters β_2. Nuclear structure effects are also evident at forward angles at the filling of the $1p$ shell. A set of mass dependent optical-model parameters which produces acceptable fits at forward angles was derived. The imaginary part was found to contain terms connected with the above structure effects. The results of this and of a coupled-channels analysis are discussed.

NUCLEAR REACTIONS Proton scattering on ^{9}Be, ^{10,11}B, ^{12,13}C, ^{14,15}N, ^{16,17,18}O, ^{19}F, ^{20,22}Ne, ^{23}Na, ^{24,25,26}Mg, ^{27}Al, ^{28,29,30}Si, ^{31}P, ^{32,34}S, ^{35,37}Cl, ^{40}Ar, ^{39,41}K, ^{40,42,43,44,48}Ca, ^{45}Sc, ^{46,47,48,50}Ti, ^{51}V, ^{50,52,53,54}Cr, ^{55}Mn, ^{54,56,58}Fe, ^{59}Co, ^{58,60,61,62,64}Ni, ^{63,65}Cu, and ^{64,66,67,68,70}Zn; E_p = 35.2 MeV. On ^{23}Na, ^{31}P, ^{39}K, ^{45}Sc, ^{51}V, ^{50,53,54}Cr, and ^{62,64}Ni at E_p = 29.7 MeV. Measured $\sigma(\vartheta)$ for elastic and inelastic scattering to 2^+_1 states. Optical-model and coupled-channel analysis. Deduced optical-model parameters and β_2 quadrupole deformation parameters.

I. INTRODUCTION

A previous study of the energy dependence of proton elastic scattering on light nuclei did evidence an enhancement of the backward angles yield which cannot be predicted by conventional optical-model calculations.[1] The same study also showed that this effect is particularly pronounced at proton energies between 30 and 40 MeV; further systematic measurements were therefore performed at an incident energy of 35.2 MeV. The data thus collected constitute a set of differential cross sections concerning nearly every stable isotope in the $A = 9-70$ mass region. Measurements were also performed at 29.7 MeV on ten nuclei, and the data on these measurements, together with those already existing in the literature,[2] form a second set involving about forty nuclei at an incident energy of 30 ± 0.3 MeV.

The measurements reported in this paper further strengthen the hypothesis advanced in Ref. 1 (hereinafter referred to as Paper I) of the existence of a correlation between proton elastic scattering and the structure of the target nuclei.

Besides elastic scattering, the analyses and phenomenological comparisons presented in the following sections also cover inelastic scattering from the first 2^+ state in even-even nuclei.

II. EXPERIMENTAL DATA

The differential cross section for proton scattering at an incident energy of 35.2 MeV was measured on the following 61 nuclei: ^{9}Be (100%), ^{10}B (19.9%), ^{11}B (80.1%), ^{12}C (98.9%, CH_4), ^{13}C (93.1%, CH_4), ^{14}N (99.6%), ^{15}N (95%), ^{16}O (99.8%), ^{17}O (75.6%), ^{18}O (95%), ^{19}F (100%, CF_4), ^{20}Ne (99.9%), ^{22}Ne (99.2%), ^{23}Na (100%, NaF), ^{24}Mg (99.9%), ^{25}Mg (99%), ^{26}Mg (98.7%), ^{27}Al (100%), ^{28}Si (92.2%), ^{29}Si (98.4%, SiO_2), ^{30}Si (88.4%, SiO_2), ^{31}P (100%), ^{32}S (95%, SF_6), ^{34}S (90%, SCd), ^{35}Cl (75.5%, CH_3Cl), ^{37}Cl (24.5%, CH_3Cl), ^{39}K (93.1%, K_2CO_3), ^{41}K (95.8%, KCl), ^{40}Ar (99.6%), ^{40}Ca (99.9%, $CaCO_3$), ^{42}Ca (76.3%, $CaCO_3$), ^{43}Ca (49.1%, $CaCO_3$), ^{44}Ca (95.8%, $CaCO_3$), ^{48}Ca (96.5%, $CaCO_3$), ^{45}Sc (100%), ^{46}Ti (98%, Ti, TiO_2), ^{47}Ti (66.2%, TiO_2), ^{48}Ti (99.9%, Ti, TiO_2), ^{50}Ti (57.6%, TiO_2), ^{51}V (100%), ^{50}Cr (90%), ^{52}Cr (99.8%, CrO_3), ^{53}Cr (95%), ^{54}Cr (94%), ^{55}Mn (100%), ^{54}Fe (95%), ^{56}Fe (91.7%), ^{58}Fe (71.5%), ^{59}Co (100%), ^{58}Ni (99%), ^{60}Ni (99%), ^{61}Ni (94.8%), ^{62}Ni (90%), ^{64}Ni (90%), ^{63}Cu (99.8%), ^{65}Cu (99.7%), ^{64}Zn (99%), ^{66}Zn (96.1%), ^{67}Zn (78.6%), ^{68}Zn (99.0%), and ^{70}Zn (90%). The numbers in parentheses for each nucleus give the isotopic enrichment of the target. The chemical form is also given, except for targets of pure elements.

A second group of measurements at 29.7 MeV

involved the following nuclei: ^{23}Na, ^{31}P, ^{39}K, ^{45}Sc, ^{51}V, ^{50,53,54}Cr, and ^{62,64}Ni.

A description of the experimental setup is given in Paper I, while the numerical data and errors are collected in an *ad hoc* report.[3] Gaseous targets allow greater precision in the determination of the values of the target density and therefore of the relative cross sections for different nuclei. For this reason gaseous targets were used whenever possible (14 nuclei), while for other nuclei self-supporting metal foils of uniform thickness were utilized. When solid targets in this form were not available or were too difficult to obtain, chemical compounds deposited on a plastic film were used. In these cases (14 nuclei) we usually obtained cross section values relative to some other nucleus, generally ^{16}O, contained in the chemical compound. A plastic film of Moplefan $(C_3H_4)_n$, which does not contain oxygen, was used as backing. The isotopic enrichment was generally more than 90%. For some nuclei (^{17}O, ^{30}Si, ^{42,43}Ca, ^{47,50}Ti, ^{58}Fe, and ^{67}Zn) the enrichment was smaller but the percentage of the various isotopes contained in the target was known. In these cases several targets were used, as many as the isotopes studied but with a different isotope content, and at the angles where the elastic peaks merge isotopic cross sections were obtained as the

TABLE I. Data concerning the even-even nuclei considered in the present study. Information on the accuracy of the cross-section measurements is given in the second and third columns. The target groups *A*, *B*, *C*, and *D* correspond to different counter setups. Relative errors within a given group are smaller (see text). The errors relative to ^{16}O are 1.7, 3, and 4.2% for nuclei belonging to groups *A*1, *A*2, and *A*3, respectively. Column 4 gives the peak values at the backward maximum of the differential elastic cross section. Their inverse are given in the last column to facilitate comparison with the quadrupole deformation parameters deduced from electromagnetic transitions β_2^{em} and from inelastic scattering β_2^{in}. The superscript letters (a to e) on β_2 values correspond, respectively, to Refs. 7 to 11.

Nucleus	Target group	Systematic error (%)	σ_{peak} (mb/sr)	$\lvert\beta_2^{em}\rvert$	β_2^{in}	$0.1/\sigma_{peak}$
^{12}C	*A*1	3.6	0.30–0.37	0.600 [a]	–0.60	0.27–0.33
^{16}O	*A*1	3.6	0.57	0.350 [a]	0.25	0.175
^{18}O	*A*1	3.6	0.22	0.320 [a]	0.39	0.454
^{20}Ne	*A*1	3.6	0.09–0.12	0.728 [d]	0.60	0.83–1.17
^{22}Ne	*A*1	3.6	0.14–0.17	0.590 [c]	0.49	0.59–0.71
^{24}Mg	*B*	4.6	0.11–0.14	0.640 [c]	0.48	0.71–0.91
^{26}Mg	*C*	4.6	0.25	0.520 [b]	0.36	0.40
^{28}Si	*D*	6.1	0.23–0.26	0.400 [b]	–0.40	0.38–0.43
^{30}Si	*A*2	5.0	0.28	0.320 [a]	–0.33	0.35
^{32}S	*A*1	3.6	0.34	0.320 [c]	0.32	0.30
^{34}S	*B*	7.0	0.40	0.260 [c]		0.25
^{40}Ar	*A*1	3.6	0.31	0.310 [c]	–0.25	0.33
^{40}Ca	*A*2	6.1	0.63	0.117 [d]		0.16
^{42}Ca	*A*2	5.0	0.34	0.244 [d]	0.24	0.30
^{44}Ca	*A*2	5.0	0.31	0.253 [d]	0.24	0.33
^{46}Ti	*A*2	4.6	0.35	0.290 [b]	0.28	0.29
^{48}Ca	*A*2	5.0	0.44	0.102 [d]	0.16 [e]	0.23
^{48}Ti	*A*2	5.0	0.37	0.265 [b]	0.25	0.27
^{50}Ti	*A*2	5.0	0.41	0.175 [b]	0.19	0.24
^{50}Cr	*B*	8.8	0.46	0.292 [d]	0.24	0.22
^{52}Cr	*A*2	5.0	0.53	0.225 [d]	0.18	0.19
^{54}Cr	*B*	8.8	0.32	0.270 [d]	0.20	0.31
^{54}Fe	*B*	4.6	0.58	0.180 [b]	0.16	0.17
^{56}Fe	*D*	4.6	0.37	0.245 [d]	0.21	0.27
^{58}Fe	*A*2	4.6	0.34	0.270 [b]	0.26	0.30
^{58}Ni	*D*	8.8	0.49	0.187 [b]	0.19	0.20
^{60}Ni	*C*	4.6	0.42	0.211 [b]	–0.21	0.24
^{62}Ni	*B*	4.6	0.53	0.193 [b]	–0.19	0.19
^{64}Ni	*B*	4.6	0.56	0.192 [b]	–0.18	0.18
^{64}Zn	*B*	4.6	0.40	0.250 [b]	–0.23	0.24
^{66}Zn	*B*	4.6	0.48	0.227 [b]	–0.19	0.21
^{68}Zn	*B*	4.6	0.44	0.205 [b]	–0.19	0.23
^{70}Zn	*B*	4.6	0.40	0.229 [b]	–0.19	0.25

solution of a system of equations relative to the various targets. In two cases, those of B and Cl, targets containing the natural isotopic mixture were used. For these nuclei the quoted elastic differential cross sections correspond effectively to each single isotope only at angles large enough for kinematics to allow the resolution of the elastic peaks. These angles were 43° and 100° for boron and chlorine isotopes, respectively.

For most nuclei the absolute cross sections were deduced directly on the basis of integrated beam current, the target thickness and the solid angle. The uncertainty in the cross sections for each point in the angular distribution is due to statistical and systematic errors. Counting statistics give sizeable contributions only at backward angles. For elastic scattering the statistical error is generally smaller than 4% even in the minima of the angular distributions at backward angles. Systematic errors result from several causes. The absolute uncertainties due to beam current integration and dead time corrections are very small being of the order of 0.2% and less than 1%, respectively. The error due to the uncertainty in the determination of solid angles reaches a maximum value of the order of 1.5% for solid and 3% for gaseous targets. This error becomes negligible, however, if relative values considered are of cross section taken with the same counter set-up (same target group as in Tables I and II). The uncertainty in the measurement of target thickness and uniformity is of the order of 3%–8% and for most solid targets constitutes the largest source of error. The effective thickness of gas targets is proportional to $nd\sin\theta$; the uncertainty in n (the number of nuclei cm^3) is estimated to be approximately 1%, while the contributions coming from d (the width of the front slit) and θ (the scattering angle) are already included in the 3% error mentioned above for the solid angle of gaseous targets. The overall systematic errors are therefore smaller for these targets than for solid ones (see Tables I and II). At small angles other systematic errors may be present. In fact the extraction of the scattering

TABLE II. Same as Table I for odd-A and odd-odd nuclei. The values reported for the quadrupole deformation parameters are derived from g.s. electric quadrupole moments β_2^Q, core excitation β_2^{ce}, and the electromagnetic parameters of the neighboring even-even nuclei β_2^{em}. The superscript letters (a to h) on the β_2^{ce} values correspond to Refs. 13 to 20. The β_2^Q values were derived from Ref. 12.

Nucleus	Target group	Systematic error (%)	σ_{peak} (mb/sr)	β_2^Q	β_2^{em}	β_2^{ce}	$0.1/\sigma_{peak}$ (mb/sr)$^{-1}$
^{9}Be	*B*	4.2	0.19–0.23	0.26			0.43–0.53
^{10}B	*B*	8.8	0.75	0.31		0.37[a]	0.13
^{11}B	*B*	8.8	0.55	0.15		0.70[b]	0.18
^{13}C	*A*1	3.6	0.55		0.47	0.41[c]	0.18
^{14}N	*A*1	3.6	0.86	0.023		0.25[c]	0.12
^{15}N	*A*1	3.6	0.68		0.35	0.28[c]	0.15
^{17}O	*A*1	3.6	0.53	0.045	0.33		0.19
^{19}F	*A*1	3.6	0.12		0.50		0.83
^{23}Na	*A*3	6.1	0.19	0.144	0.62	0.60[d]	0.53
^{25}Mg	*B*	5.3	0.27–0.30	0.20	0.54		0.33–0.37
^{27}Al	*C*	4.6	0.40	0.12	0.44		0.25
^{29}Si	*A*2	5.0	0.32		0.36	0.32[e]	0.31
^{31}P	*B*	7.0	0.33		0.31	0.28[e]	0.30
^{35}Cl	*A*1	3.6	0.46	0.040	0.25		0.22
^{37}Cl	*A*1	3.6	0.64	0.031	0.16		0.16
^{39}K	*A*2	5.0	0.60	0.023	0.14		0.16
^{41}K	*A*3	7.0	0.48	0.027	0.24		0.21
^{43}Ca	*A*2	5.0	0.44		0.25	0.25[d]	0.23
^{45}Sc	*D*	4.6	0.39	0.076	0.27	0.20[f]	0.26
^{47}Ti	*A*2	5.0	0.46	0.093	0.28	0.27[f]	0.22
^{51}V	*D*	4.6	0.47	0.014	0.20	0.25[c]	0.21
^{53}Cr	*B*	8.8	0.42	0.008	0.25		0.24
^{55}Mn	*B*	6.1	0.37	0.10	0.27	0.27[g]	0.27
^{59}Co	*D*	4.6	0.47	0.090	0.21		0.21
^{61}Ni	*C*	4.6	0.56	0.033	0.19		0.18
^{63}Cu	*B*	5.3	0.52	0.036	0.19	0.19[h]	0.19
^{65}Cu	*B*	4.6	0.47	0.038	0.20		0.21
^{67}Zn	*C*	4.6	0.51	0.031	0.20		0.20

yields is generally straightforward except for elastic peaks at forward angles, where events produced by contaminants or other nuclei (mainly oxygen) present in the target have to be separated. The data can be corrected for these spurious effects if the differential cross section of the contaminant nucleus is known, by determining its content in the target from the chemical form of the compound used or directly from the data at large angles, where the kinematics allows separation of the different elastic peaks. A further source of error is connected with uncertainties in the beam direction and counter positioning. These, estimated to be within ±0.1°, give sizable errors in the cross section where its angular dependence is very strong such as for nuclei with $A>30$ at scattering angles smaller than 40°. Typical values for total systematic errors in this case may be of the order of 10%. A tail in the spectrum of a single monoenergetic group is produced by edge effects in the slit material and by protons which undergo a nuclear reaction in the silicon detector. The fraction of elastically scattered protons lost from the peak because of the latter effect can be evaluated by using total reaction cross section values for silicon.[4] This fraction is of the order of 1.3% at 35 MeV and less than 1% at 30 MeV. The contribution of this tail to the 2^+ inelastic yield was subtracted by drawing a smooth curve through the minima in the spectra. The uncertainty resulting from this procedure is significant only at forward angles.

III. PHENOMENOLOGICAL FEATURES OF THE DATA

Several significant features emerge from a first inspection of the data. Many nuclei exhibit an enhanced yield at backward angles which is especially evident in two mass regions close to ^{16}O and ^{40}Ca. Typical angular distributions for nuclei in these regions are given in Figs. 1 and 2. Starting from ^{9}Be, the cross section at backward angles increases with the mass, reaches a maximum value for ^{14}N, and then decreases to a minimum value for ^{20}Ne. In the calcium region the largest backward yield is found for ^{40}Ca. The other nuclei with a neutron number $N=20$, i.e., ^{37}Cl and ^{39}K, give an equal yield. The backward maximum is already lowered by a factor of 1.5 for ^{35}Cl ($Z=17, N=18$) and ^{41}K ($Z=19, N=22$) and by a factor of 2 for ^{40}Ar ($Z=18, N=22$) and ^{42}Ca ($Z=20, N=22$). It therefore seems more probable that this effect is related to the structure than to the dimensions of the nucleus. Further support for this statement comes from the differences found for the isobaric pairs ^{40}Ar-^{40}Ca, ^{48}Ca-^{48}Ti, ^{54}Cr-^{54}Fe, ^{58}Fe-^{58}Ni, and ^{64}Ni-^{64}Zn, in which the closed shell nuclei (^{40,48}Ca, ^{54}Fe, and ^{58,64}Ni) show the largest backward yield. It has already been observed (see for instance Ref. 5) that a deep minimum at backward angles gives an "anomalous" shape to the angular distributions for proton elastic scattering on ^{16}O and ^{40}Ca. In the oxygen region (Fig. 1) the cross sections at scattering angles larger than 60°, and therefore also at the last minimum in the angular distribution, coherently follow the changes in the yield of the backward maximum. In the calcium region the cross section at the last minimum stays fixed (Fig. 2), while the following maximum changes with the nucleus. It therefore seems that for the effect studied here the peak cross section at the back-

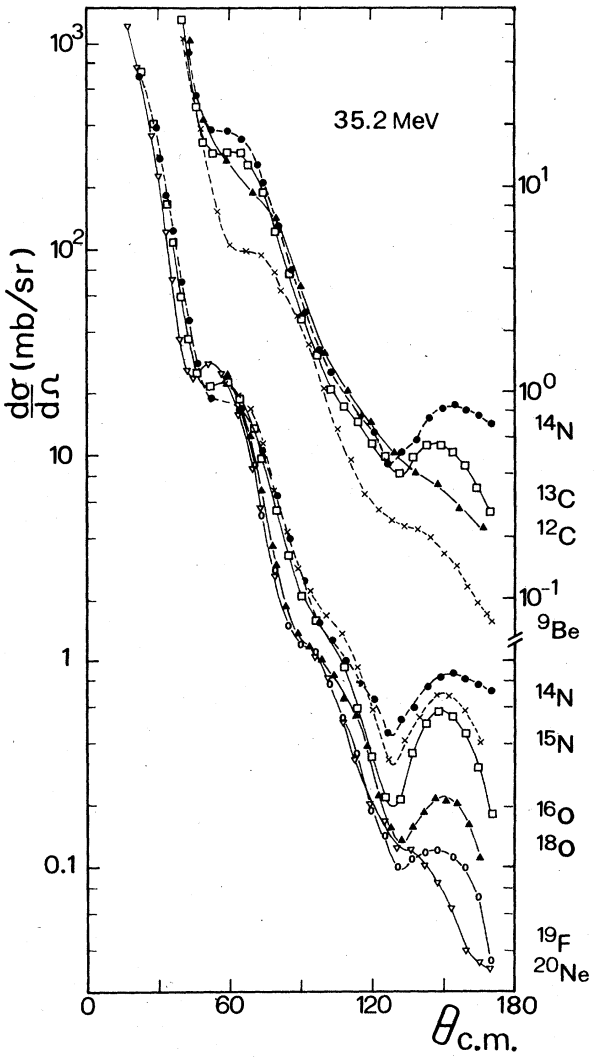

FIG. 1. Mass dependence of the backward maximum for nuclei in the ^{16}O region. Data for ^{17}O have been omitted, being very similar to those for ^{16}O. The lines drawn through the experimental points are only to guide the eye.

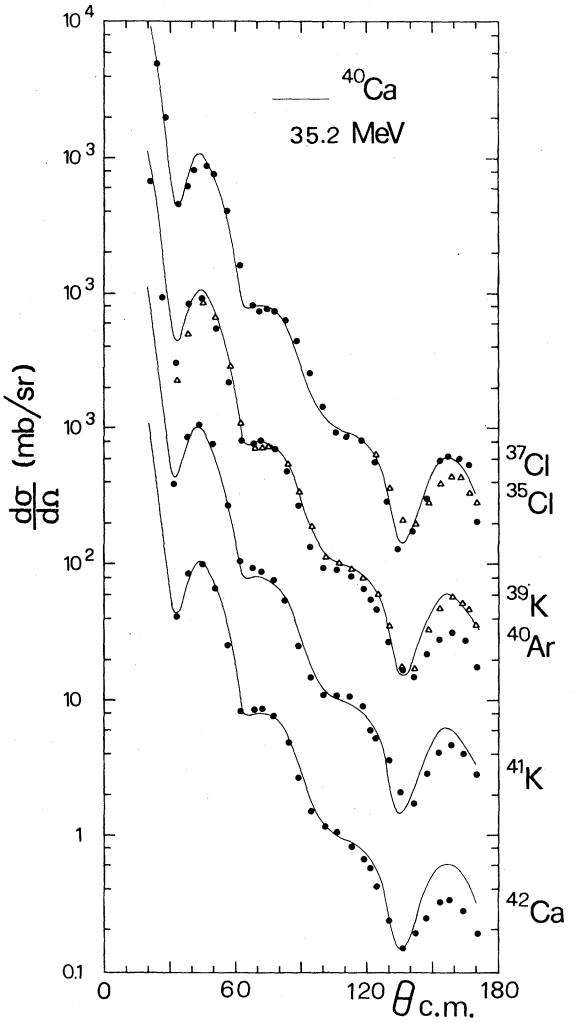

FIG. 2. Same as in Fig. 1 for nuclei in the ^{40}Ca region. The full lines are an interpolation of the ^{40}Ca data and are used as a reference for other nuclei.

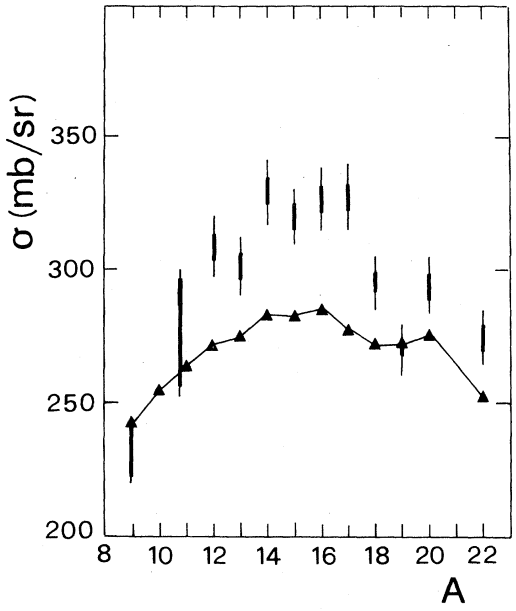

FIG. 3. Experimental cross-section values integrated between 20° and 40° with the estimated uncertainty in relative values (heavy vertical bars) compared with folding-model calculations (Ref. 6) (triangles and solid line). The fine vertical bars indicate the upper limit of the errors also taking into account the uncertainty in the absolute normalization.

ward maximum is more significant than the relative depth of the last minimum. For this reason the peak cross section value (σ_{peak}) at the backward maximum in the angular distribution is being considered in order to parametrize the effect.

It was also observed that an enhanced yield was not limited to the backward angles region mentioned above. In this respect we have so far performed a careful study on nuclei up to $A = 22$, where the effect is larger and the use of gaseous targets for several nuclei makes it possible to obtain more precisely determined relative cross section values. The cross sections integrated over the forward angles (20°–40°) are shown in Fig. 3. A comparison of Figs. 1 and 3 shows at a glance that those nuclei for which the backward effect is most enhanced, e.g., ^{14,15}N, ^{16,17}O, are also characterized by a larger forward cross section. To help judge the extent of the effect, the results of folding-model calculations[6] were used as a reference. Due to shift with the mass of the diffraction pattern within the angular interval chosen (20°–40°), these results show a similar but less pronounced increase for the same nuclei. The size of the effect can then be judged by comparing the calculated with the more marked experimental mass dependence. Although the forward effect attains sizable absolute values (judging from Fig. 3 it is at least of the order of 50 mb) it is relatively less important than the effect at backward angles and for this reason can be easily reproduced by standard optical-model calculations with only minor adjustments in the parameters.

The σ_{peak} values at 35.2 MeV for the nuclei studied here are given in Tables I and II and are plotted against the mass number together with those at 30 MeV in Fig. 4. The overall trend at the two energies is very similar. The mass dependence of the angular position of the backward maximum is displayed in Fig. 5; the maximum shifts toward larger angles when the enhancement in the backward yield is present. The general trend of the data plotted in Figs. 4 and 5 evidences a correlation with shell closures at $N, Z = 8$ and 20. This enhancement is completely absent in ^{12}C and ^{24}Mg, studied in Paper I, as it is in other strongly de-

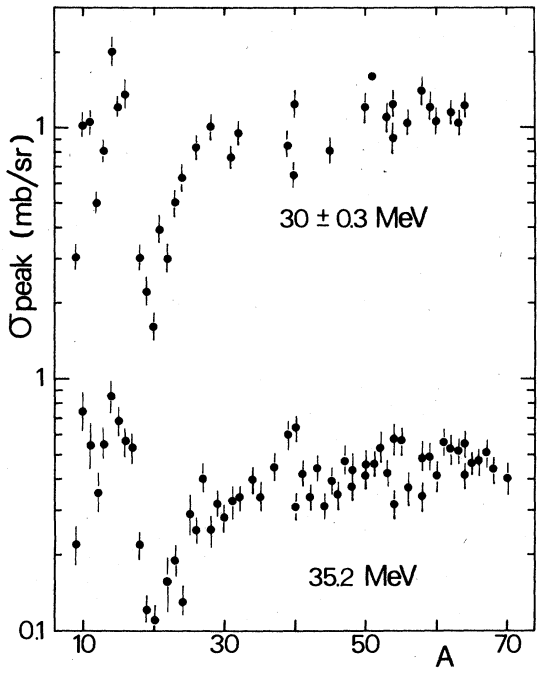

FIG. 4. Mass dependence of the peak value of the cross section at the backward maximum in the angular distribution σ_{peak} for elastically scattered protons at two energies. The error bars take into account both statistical and estimated absolute uncertainty.

formed nuclei like the neon isotopes. Spurred by this evidence, we made several attempts to find out if there is any quantitative correlation with collective properties of the target nuclei. Striking results were obtained in the comparison between the elastic scattering cross sections at backwards angles σ_{peak} and β_2, the quadrupole deformation parameter. The latter was deduced for even-even nuclei from electromagnetic transition rates[7-10] (β_2^{em} in Table I). When the cross section is expressed in mb/sr, with the exception of ^{12}C, $^{16,18}O$, and $^{40,48}Ca$, the values of $0.1/\sigma_{peak}$ are almost exactly the same as the numerical values of β_2^{em} [Fig. 6(a)] at least within the estimated errors. These

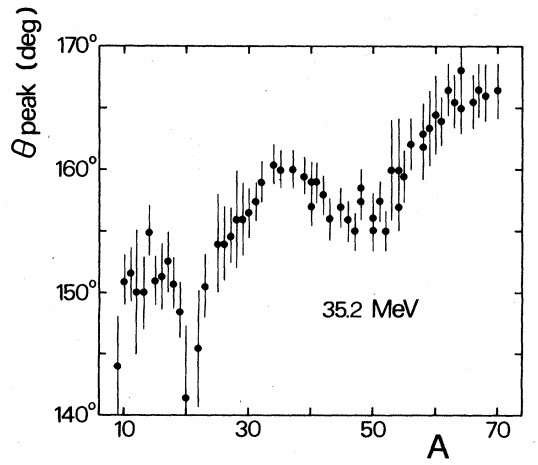

FIG. 5. Mass dependence of the angular position of the backward maximum of Fig. 4. The error bars give an upper limit to the estimated uncertainty.

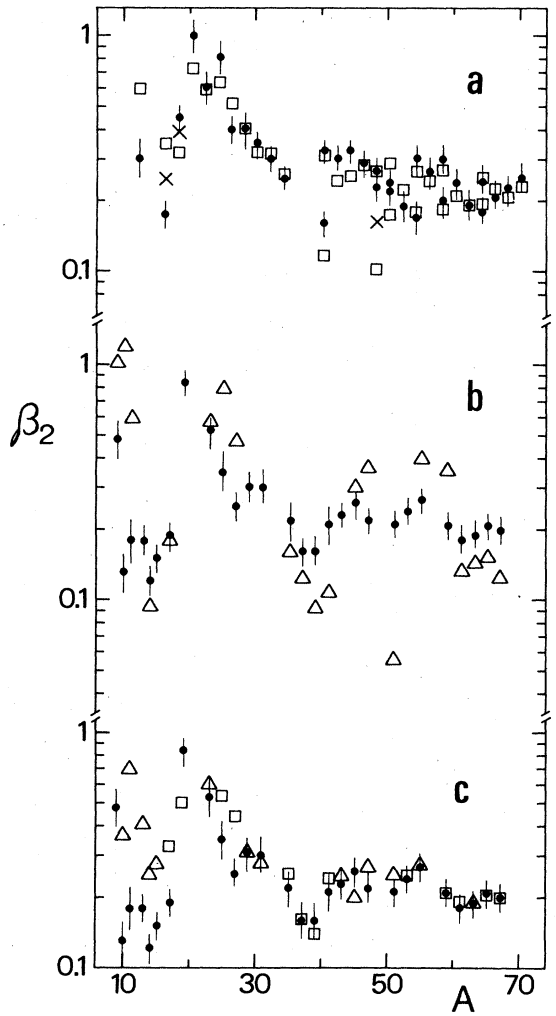

FIG. 6. Comparison of σ_{peak} and quadrupole deformation parameter values. The dots with error bars give the numerical values of $0.1/\sigma_{peak}$ (peak cross section in mb/sr). (a) Comparison for even-even nuclei. The β_2 values are deduced from electromagnetic transition rates (squares). For $^{16,18}O$ and ^{48}Ca the values obtained from inelastic scattering cross sections are also given (crosses). (b) Comparison for odd-A nuclei. The values of $4\beta_2$ deduced from g.s. quadrupole moments are given by triangles. (c) Same data as in (b) compared with β_2 values deduced from core excitation strength (triangles) or from electromagnetic properties of neighbouring even-even nuclei (squares).

are generally of the order of 5% and 10% for β_2^{em} and σ_{peak}, respectively. Better agreement for the nuclei ^{16,18}O and ^{48}Ca is obtained if the β_2 deduced from inelastic scattering are used (present experiment and Ref. 11). For these nuclei, in fact, contrary to what is generally found, the deformation parameters from inelastic scattering differ from those deduced from electromagnetic transition rates (see Sec. V and Table I). The β_2 values for odd-A nuclei and odd-odd nuclei (^{10}B and ^{14}N) are usually deduced from the ground state electric quadrupole moments[12] and are therefore related to the ground state static deformations. The A-dependence gross structure of the β_2^0 is still reproduced [Fig. 6(b)] but less satisfactorily and with a different relative normalization ($0.1/\sigma_{peak} \simeq 4\beta_2^0$). For several odd nuclei considered herein it has been shown[13-20] that the low-lying levels can be described by coupling the extra particle or hole to collective states of an even-even core and that the collective excitation of the low-lying multiplets has a strength which corresponds to that of the parent 2_1^+ state in the neighboring nucleus. If we use the β_2^{ce} derived from these core excitations or, for lack of data, the β_2^{em} of the neighboring even-even nuclei, the agreement found for even-even nuclei is also obtained for odd-A nuclei [Fig. 6(c)]. The results of the above comparisons can then be summarized with the assertion that a correlation, which can hardly be fortuitous, has been found and that it indicates that at 30–40 MeV the proton elastic scattering is strongly affected by collective couplings.

These findings could suggest that coupled-channels calculations may be needed to fit the elastic scattering cross sections. Owing to the above correlation with the β_2 parameters, couplings that obviously should be considered are those within the ground state rotational or vibrational bands. Calculations of this type have been attempted but have given rather unsatisfactory results, as could have been predicted. In fact the coupling to collective low-lying states in strongly deformed nuclei can produce sizeable effects in the elastic channel; for these nuclei, however, the elastic scattering is already satisfactorily reproduced by simple optical-model calculations. For this reason the parameters deduced in optical-model analyses are usually readjusted in coupled-channels calculations to restore, or in more favorable cases to slightly improve, the agreement with experimental elastic scattering cross sections. On the other hand, it can be readily seen (see Sec. V) that in a spherical nucleus the weak coupling between the ground state and the low-lying excited states does not give rise to any enhancement of the cross section at backward angles.

IV. OPTICAL-MODEL ANALYSIS

It was shown in Paper I that conventional optical-model calculations provide an acceptable fit to proton elastic scattering data for light nuclei, with the exception of the cross section at backward angles on spherical nuclei. It was also found that several parameters of the average energy dependent optical-model potentials obtained in Paper I as the result of analysis of proton elastic scattering on seven nuclei with mass numbers between 12 and 40 change regularly with energy and mass. The geometry for the imaginary and the spin-orbit wells was found to be practically mass independent, while the radius and the diffuseness parameters for the real well were found to increase fairly regularly with the mass.

To better ascertain the mass dependence of the optical parameters and to get more detailed information about the variation of the well depths with the mass, which especially for the imaginary terms is not immediately evident, we performed systematic analysis of all the 35.2 MeV data. This analysis may be considered as a possible parametrization of the experimental data, rather than an attempt to obtain average optical-model potentials to be used in further calculations. However, as shown below, part of the results of the present analysis can be supported or explained by recent calculations based on folding models which take into account only average nuclear properties and therefore give potentials which are not strictly related to the structure of each particular nucleus.

Conventional form factors were used for the optical-model potentials and only data up to 100°–130° were considered in order to remove the backward maximum in the angular distributions from the best-fitting procedure. In this respect it should be pointed out that Paper I showed how inclusion of all the angles leads to the dominance by backward angles in the least-squares search and, very often to nonphysical values for some parameters.

Starting parameters in the fitting procedure were interpolated from those given in Table II of Paper I; all the parameters were then allowed to be routinely in search in groups of 4 or 5. The spin-orbit term was searched on only in the first step of the fitting procedure and was subsequently fixed at $V_{so} = 5.6$ MeV, $R_{so} = 1.01$ fm, and $a_{so} = 0.60$ fm. These values fall in the middle of the range of those given in Paper I and in a recent study of polarization in proton elastic scattering on light nuclei at 30 MeV.[21] Our results for the mass dependence of the geometrical parameters of the real central term are shown in Fig. 7. Large fluctuations are evident for the diffuseness over the full mass range and also for R_0 below $A = 40$. The deformed

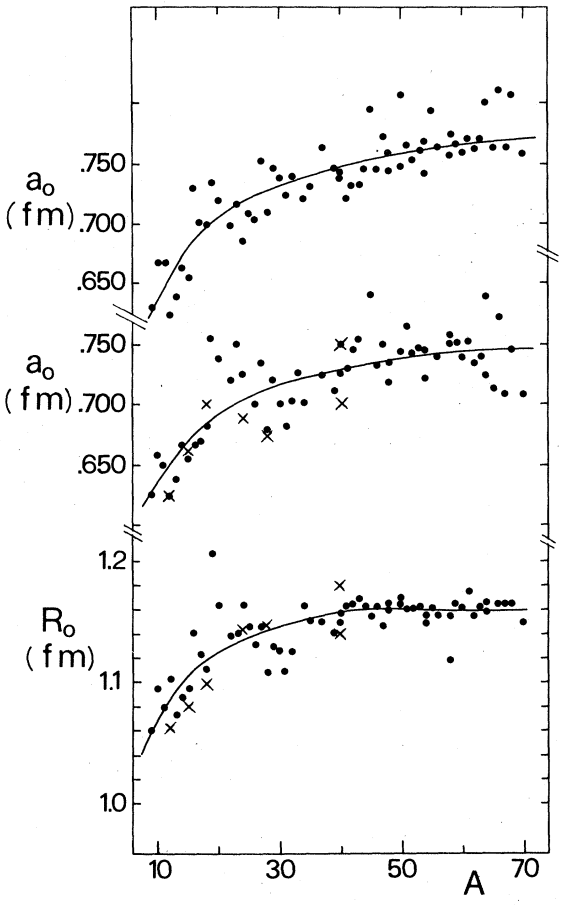

FIG. 7. Dependence on mass number of the best-fit geometrical parameters of the real part of the optical-model potential resulting from the analysis of 35.2-MeV proton elastic scattering at forward angles ($\vartheta < 100°$–130°). The two different results for the diffuseness a_0 were obtained by following two different best-fit procedures. The solid lines give a smooth interpolation of the points with the following A dependence: $a_0 = 0.819 - 0.841\,A^{-2/3}$ fm; $a_0 = 0.79 - 0.721\,A^{-2/3}$ fm and $R_0 = 1.216 - 0.674\,A^{-2/3}$ fm ($R_0 = 1.16$ fm for $A > 42$). The crosses give the values of the average energy-dependent potentials of Paper I.

nuclei in the Ne-Mg region show a preference for large values of the radius and the diffuseness. On the contrary, nuclei lighter than oxygen require small values of the same parameters. These best-fit values, as shown in Fig. 7, can be interpolated by a smooth mass dependence without a noticeable worsening of the quality of the fits and, if the well depth is readjusted, with no appreciable change in the volume integrals per nucleon J_v/A. The radius parameter was therefore interpolated using the relationships $R_0 = 1.216 - 0.674A^{-2/3}$ fm and $R_0 = 1.16$ fm for $A \geq 42$. The latter value is very similar to the one given by Becchetti and Greenless.[22] To understand this result found for the mass dependence of the radius it can be recalled that the convolution of a nucleon-nucleon force of range t on a Woods-Saxon mass distribution of half-density radius C_v results in a folded potential also of a Woods-Saxon shape with a radius given by[23,24]:

$$\bar{C}_v = C_v\left(1 - \frac{t^2}{2C_v^2}\right)$$

This formula is sufficiently exact for $t/C_v \ll 1$ and is also still acceptable for light nuclei. If one takes $C_v = R_0 A^{1/3} = (k_1 + k_2 A^{1/3})A^{1/3}$ fm as has been done for proton distributions,[24,25] one obtains a mass dependence for the radius of the potential distribution of the following type:

$$\bar{C}_v = \bar{R}_0 A^{1/3} = (a + bA^{1/3} - cA^{-2/3} \cdots)A^{1/3}\ \text{fm}.$$

Both mass-dependent terms lead to an increase of $\bar{R}_0$ with A. The term in $A^{-2/3}$ is dominant for small A values. The best-fit values for the diffuseness can be interpolated by a similar mass dependence: $a_0 = 0.79 - 0.721A^{-2/3}$ fm. This last result is more strongly affected than that for R_0 by the best-fit procedure (groups of parameters searched on and their sequence). It can however be stated without any ambiguity or uncertainty that heavier nuclei require larger diffuseness values.

The root mean squared (rms) radii $\langle r^2 \rangle^{1/2}$ obtained in the present analysis are shown in Fig. 8(c); they agree with those given in folding-model calculations done by Jeukenne *et al.*,[24] also given in the figure.

The real well depth best-fit values, as resulting from the present analysis with geometrical parameters fixed at the above values, give the volume integrals per nucleon J_v/A shown in Fig. 8(a). These are compared with the dependence (full curve) given by the folding-model calculations of Ref. 24. The best-fit values of the well depth can be interpolated by

$$V_0 = 43.4 + 18.6(N - Z)/A + 0.4\,Z/A^{1/3} + 825/A^2\ \text{MeV}.$$

The symmetry term was obtained by averaging the $(N - Z)/A$ dependence for groups of isotopes and isobars; the value of the Coulomb term was taken as being equal to that used in standard potentials. The last term, which is not present in the usual form of optical-model potentials, was introduced to account for the average mass dependence of V_0 and of the real volume integral, and can be justified in a folding-model calculation. In fact for a light nucleus the low-density surface region is relatively more important so that the density dependence of nuclear forces results in larger values for the strength of the nucleon-nucleus interaction. It should be noted in this connection that the volume integral per nucleon, as shown in Fig. 8, de-

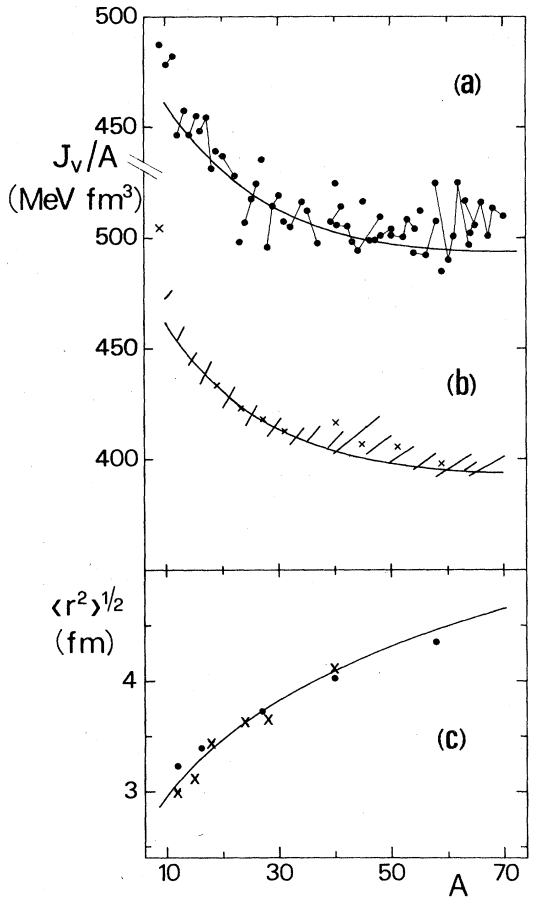

FIG. 8. (a) Dependence on mass number of the volume integrals per nucleon of the real part of the potential in Fig. 7. The dots give the results of the best-fit procedure with geometrical parameters fixed at the interpolation values of the Fig. 7 and well depths searched on. The points belonging to the same group of isotopes are connectted by lines. The smooth solid line gives the result of a folding-model calculation (Ref. 24). (b) Volume integral per nucleon of the real part of the average mass-dependent potential given in Sec. IV (straight lines and crosses) compared with the same folding-model calculations as in (a). (c) Mass dependence of the rms radius of the real part of the potential of (b) (solid line) compared with folding-model calculations as in (a) for ^{12}C, ^{16}O, ^{28}Si, ^{40}Ca, and ^{58}Ni (dots) and values from the average energy-dependent potentials of Paper I for ^{12}C, ^{15}N, ^{18}O, ^{24}Mg, ^{28}Si, ^{40}Ar, and ^{40}Ca (crosses).

creases by about 20% in going from $A=9$ to $A=70$. Considering that for a Woods-Saxon distribution the volume integral per nucleon is given approximately by

$$\frac{4\pi}{3}V_0R_0^{\,3}\left[1+\left(\frac{a_0\pi}{R_0A^{1/3}}\right)^2\right]$$

and taking the average mass-dependent values for V_0, R_0, and a_0 given above, it is found that the strength V_0 and the geometrical factor have approximately an equivalent effect on the above decrement. If a potential is used with fixed geometrical parameters and a strength V_0 with only the small mass dependence arising from the Coulomb and symmetry terms,[22] a mass variation is obtained which is almost due only to the volume per nucleon and which is too large (30%–40% in our mass range). These two possible sources of mass dependence, the volume and the strength V_0 are practically indistinguishable in the analysis of elastic scattering data on medium-weight nuclei but can be separated in the analysis of light nuclei. It is interesting to observe again that the mass dependence of global properties, such as the rms radius and the volume integrals, obtained in the analysis of data for light nuclei is in good agreement with theoretical folding-model predictions.

The analysis of the mass dependence of the absorptive part of the optical-model potential is less straightforward. If the imaginary terms are described with four parameters (the two well depths W_v and W_D for the volume and surface terms, the radius R_w and the diffuseness a_w) and these parameters are freely searched on, results like those shown in Fig. 9 are obtained. Strong fluctuations are present over the whole mass range. The fluctuations of the two well depths W_v and W_D in most cases are correlated and out of phase. The same is found for the fluctuations of the geometrical parameters R_w and a_w which do not seem to be systematically correlated with any physical property of the target nucleus. Moreover there is no evidence for the commonly accepted isospin dependence of the diffuseness. For this reason, fixed average values have been used for both the radius, set equal to $R_w=1.252$ fm and the diffuseness, set equal to $a_w=0.678$ fm. Again, as for the real term, if the well depths are readjusted, the use of fixed geometrical parameters gives rise to only minor changes in the values of χ^2 and of the volume integrals J_w/A. The strong fluctuations noted above in the values of the well depths W_v and W_D are not eliminated, however.

A symmetry component is clearly present in the volume integrals as can be seen in Fig. 10(a). The lines which connect the best-fit values of the imaginary volume integral for groups of isotopes generally have a positive slope with increasing mass. This behavior indicates the presence of a $W_1(N-Z)/A$ term coherent with the isoscalar part of the imaginary optical potential. A similar indication can be derived from the isobaric pairs. The presence of this term in the mass dependence of each single well depth W_v and W_D is less evident. Closer analysis of the correlation between the values of the imaginary depths and the values of $(N-Z)/A$ indi-

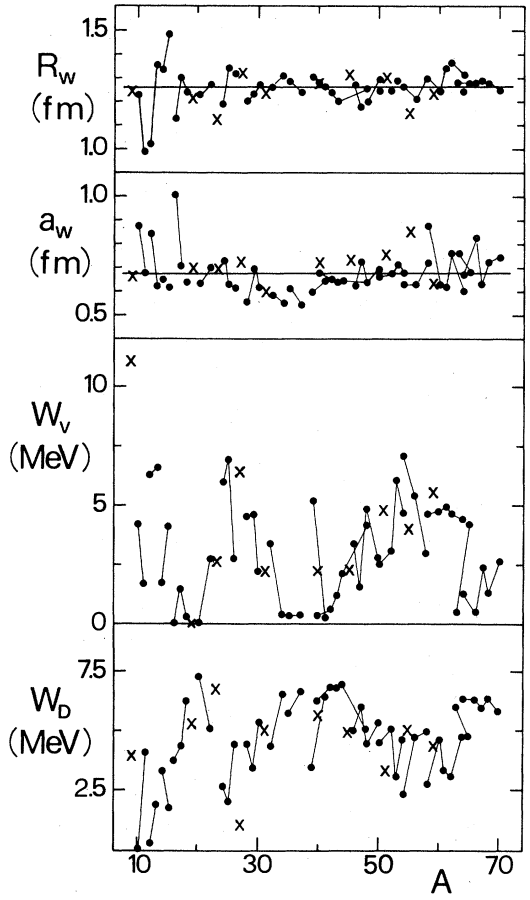

FIG. 9. Mass dependence of the parameters for the imaginary terms of the optical potential. The lines connect values corresponding to groups of isotopes, the crosses indicate elements for which only one isotope has been investigated.

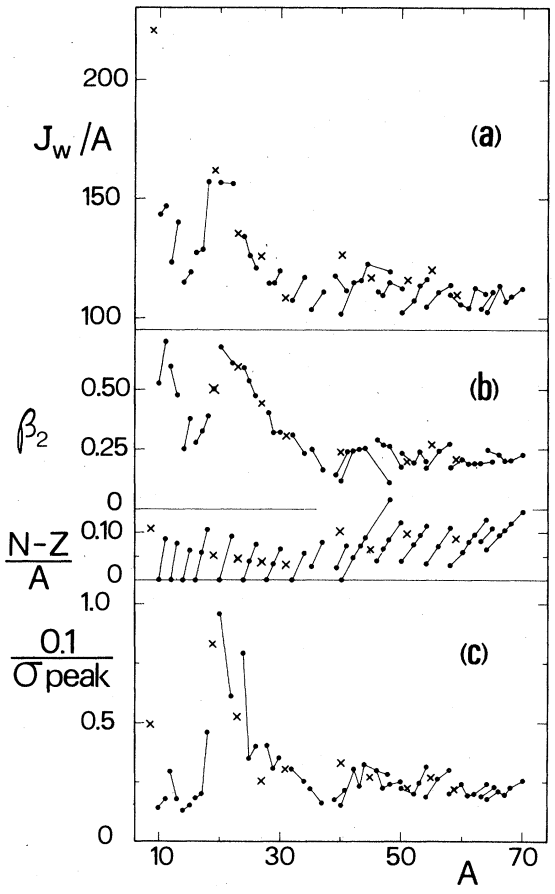

FIG. 10. (a) Mass dependence of the volume integrals per nucleon of the imaginary term of the optical potential. The geometrical parameters have been fixed at the average values ($R_w = 1.252$ fm, $a_w = 0.678$ fm) and the well depth of the volume and surface term has been searched on. The points connected by lines belong to the same group of isotopes; the crosses indicate elements for which only one isotope has been investigated. (b) Deformation parameters derived from electromagnetic transitions β_2 and $(N-Z)/A$ values. (c) Values of $0.1/\sigma_{peak}$.

cates that this symmetry term should probably be included in the surface potential. A gross structure is present in the J_w/A mass dependence underlying the symmetry component which represents a sort of fine structure. This gross structure, as shown in Fig. 10, is very similar to that displayed by the mass dependence of the deformation parameters β_2^{em}. In Fig. 10(c) the values are given for $0.1/\sigma_{peak}$, where σ_{peak} is the value of the cross section on the maximum at backward angles. It is interesting to remark that the volume integrals, which are obtained from an optical-model analysis of the forward angle data, are correlated with collective properties in the same way as the backward angle cross sections. This is further proof that nuclear structure effects, which are so evident at backward angles, are also present in the full angular distribution. Additional indications can be gathered from more detailed analysis of the results shown in Fig. 10: The dependence of the symmetry term is more evident in J_w/A than in σ_{peak}, and the trend of the former is in good agreement with that of $0.1/\sigma_{peak}$ except for light nuclei ($A<16$). In this region there is better agreement with β_2^{em}. It should be recalled that the correlation between β_2^{em} and $0.1/\sigma_{peak}$ is worse for these nuclei.

It is very difficult to reproduce the trend of W_v, W_d, and J_w/A at the same time with an average potential since it is not clear how to unfold the volume and surface contributions in J_w/A found in the best-fit procedure. Good agreement with the J_w/A mass dependence and fairly good correspondence with the results for W_D are obtained by assuming a fixed value for W_v (3.7 MeV) and taking

$$W_D = 7(N-Z)/A + (1.1\beta_2 + 0.9)A^{1/3}\ \text{MeV},$$
$$= 7(N-Z)/A + (0.11/\sigma_{\text{peak}} + 0.9)A^{1/3}\ \text{MeV}.$$

This choice results in a sizable increment (by a factor of about 2) of the overall χ^2 value in comparison with the one obtained by a free search on W_v and W_D. The quality of the fits at forward angles is still acceptable (see Fig. 11) and the values of J_w/A are reproduced within 2%.

Folding-model calculations for ^{28}Si, ^{40}Ca, and ^{58}Ni at 30.3 MeV proton energy have been performed by Geramb *et al.*[26] Their results for J_w/A should also hold true at 35.2 MeV since the predicted energy dependence[24] of this quantity is very small around 30 MeV. The agreement with our results is satisfactory as shown in Fig. 12(a). In the same figure the results of calculations made by Jeukenne *et al.*[24] are also reported as an example of the average mass dependence given by folding-model calculations. There is no agreement with our results in the absolute values although the average trend is well reproduced.

The framework offered by the optical model may be used to relate other independent experimental data to elastic scattering. Several total reaction cross section (σ_R) measurements concerning light nuclei are reported in the literature.[27-31] Very few have been performed at 35 MeV, but the energy dependence of σ_R has been determined for several nuclei. It is therefore possible to obtain from the latter an interpolated value at 35 MeV for the following nuclei: ^{9}Be, ^{11}B, ^{12}C, ^{16}O, ^{19}F, ^{27}Al, ^{28}Si, ^{40}Ca, and ^{48}Ti. These data are shown in Fig. 12 together with the results of calculations in which

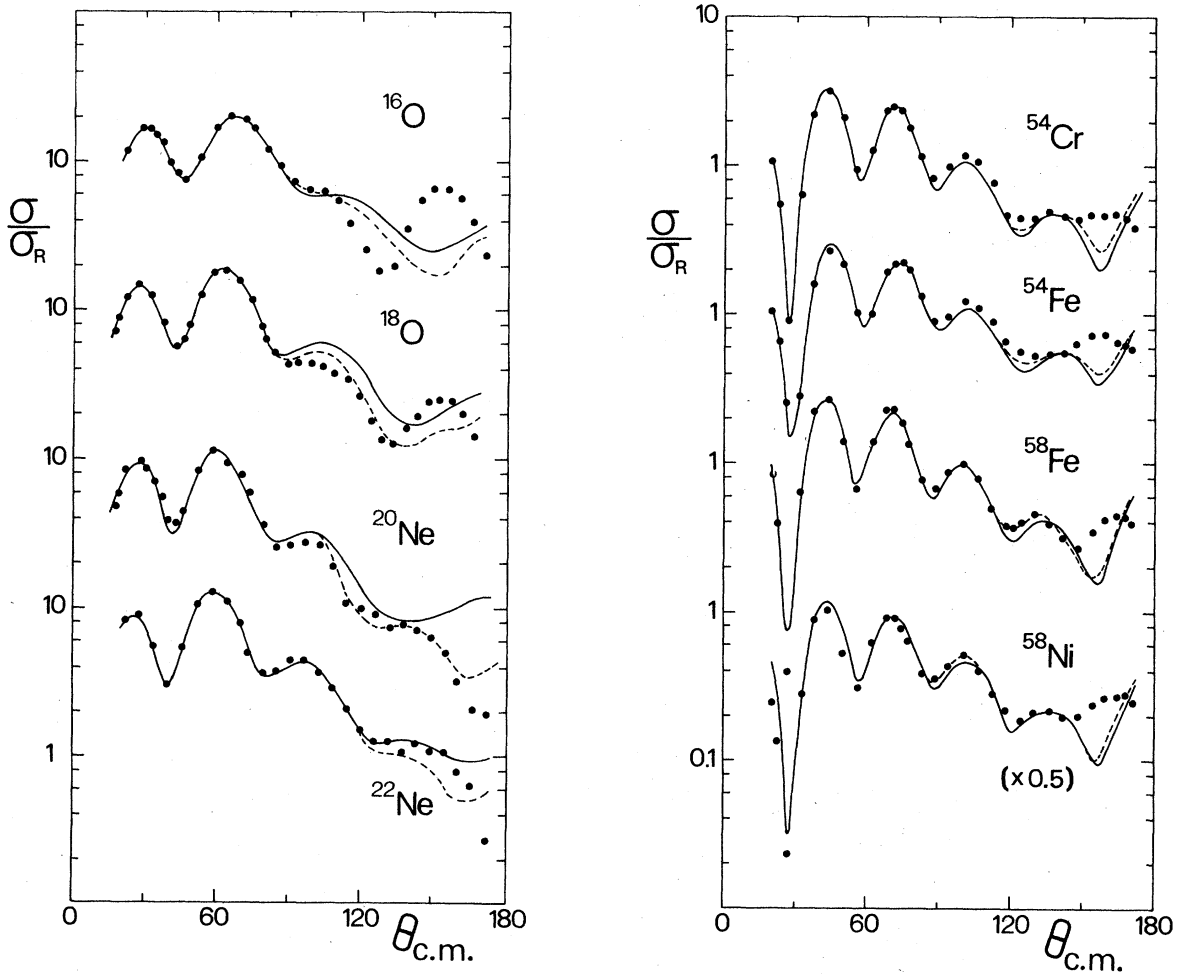

FIG. 11. Typical fits to proton elastic scattering cross sections. The solid lines are the result of the optical-model calculations with the average, mass and β_2-dependent potential given in Sec. IV. The dashed lines are the result of coupled-channel calculations for elastic and inelastic scattering to the first 2^+ excited state. Well depths both for the real and imaginary parts and β_2 values were searched on in a fit to the full angular distribution.

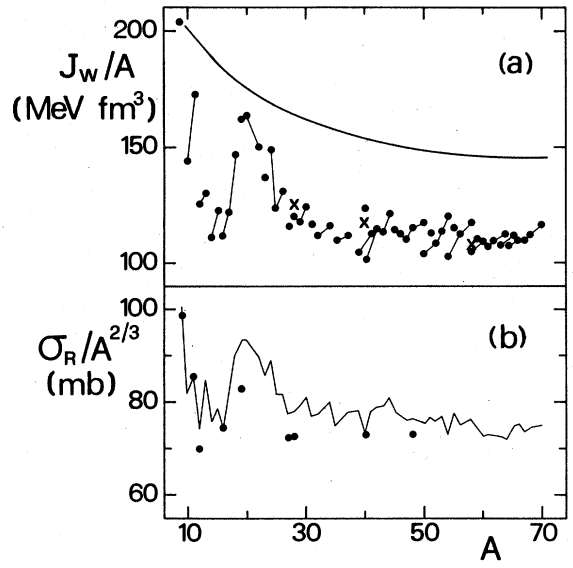

FIG. 12. (a) Volume integral per nucleon of the imaginary part of the potential given in Sec. IV. The surface well depth W_D includes the dependence on σ_{peak}. The results of the folding-model calculations of Refs. 26 and 24 are given by crosses and the solid line, respectively. (b) Total reaction cross sections calculated with the potential of (a) compared with the values obtained by interpolation of the experimental data of Refs. 27–31.

the above β_2-dependent potential was used. The similarity between the mass dependence of experimental and calculated cross sections is evident. The $1p$-shell closure produces a decrement of the flux in the reaction channels of the order of 10%–15%. This effect, which is complementary to that found in the elastic channel at forward angles (see Fig. 3), can still be reproduced by optical-model calculations. Since the mass dependence of J_w/A and therefore that of the calculated reaction cross sections are very similar to that of quadrupole deformation parameters, a parametrization of the effect can be obtained in terms of β_2 values. From this point of view, the nuclear structure effect on total reaction cross sections and on integrated elastic cross sections is connected to that found for the elastic scattering at backward angles. There are, however, at least two remarkable differences. The first, as already pointed out, is the order of magnitude of the effect; the ratio of the cross sections for ^{14}N and ^{20}Ne is 1.13 at forward angles, while it is about 8 on the backward maximum. The second difference concerns the energy dependence. In fact, while the backward effect is more evident above 26 MeV, the effect on σ_R values and on elastic scattering at forward angles and therefore in the J_w/A, deduced from the optical-model analysis is clearly also present in the 20–25 MeV energy region. This may be evidenced by the same data mentioned above for total reaction cross sections and by the optical-model analyses of Paper I and of Refs. 2, 32, and 33. For instance, the volume integrals J_w/A in the energy interval between 20 and 25 MeV are between 90 and 120 MeV fm^3 for ^{14,15}N and ^{16}O, while they reach a value of about 150 for ^{18}O and ^{20,22}Ne and of 130–135 MeV fm^3 for ^{12}C. As at higher energies the J_w/A minimum for ^{16}O and the nitrogen isotopes is a consequence of the maximum in the elastic yield for the same nuclei and is in agreement with a minimum for the experimental reaction cross sections.

The present optical-model analysis leads to the conclusion that, as found in Paper I for the energy dependence, also the mass dependence of proton elastic scattering on light nuclei can be reproduced with conventional potentials. The set of average mass-dependent parameters which has been derived is listed in Table III. The agreement between the experimental and calculated angular distributions is however generally satisfactory only up to $\vartheta = 100°$ for very light nuclei and up to $\vartheta = 150°$ for nuclei heavier than calcium. The above potential is characterized by two features not found in the hitherto available phenomenological potentials for proton scattering on medium-weight nuclei[22]: the mass dependence of the real part and the nuclear structure dependence of the imaginary part. The former can be explained by folding-model calculations, while the latter can be parametrized in terms of the quadrupole deformation parameters.

TABLE III. Optical model parameters. The potential listed is of the form

$$U(r) = -V_0 f(x_0) - i\left(W_v f(x_w) - 4W_D \frac{df(x_w)}{dx_w}\right) + \left(\frac{\hbar}{m_\pi c}\right)^2 \frac{V_{so}}{r}\frac{df(x_{so})}{dx_{so}} + V(r, R_c),$$

where $f(x_i)$ is a Woods-Saxon form factor with $x_i = (r - R_i A^{1/3})/a_i$ and where $V(r, R_c)$ is the Coulomb potential of a uniformly charged sphere of radius $R_c = 1.2A^{1/3}$.

$$V_0 = 43.4 + 18.6\frac{N-Z}{A} + 0.4\frac{Z}{A^{1/3}} + 825A^{-2} \text{ (MeV)}$$

$$R_0 = 1.216 - 0.674A^{-2/3} \text{ (fm)}$$

$$a_0 = 0.790 - 0.721A^{-2/3} \text{ (fm)}$$

$$W_v = 3.7 \text{ (MeV)}; \quad W_D = 7\frac{N-Z}{A} + (1.1\beta_2 + 0.9)A^{1/3} \text{ (MeV)}$$

$$R_w = 1.252 \text{ (fm)}; \quad a_w = 0.678 \text{ (fm)}$$

$$V_{so} = 5.6 \text{ (MeV)}; \quad R_{so} = 1.01 \text{ (fm)}; \quad a_{so} = 0.600 \text{ (fm)}$$

V. INELASTIC SCATTERING

This section contains a brief discussion of the results obtained in the present experiment for inelastic transitions to low-lying states of the residual nuclei. Particularly interesting are those to the first 2^+ excited level in even-even nuclei. In fact these states are known to be strongly coupled to the ground state and in a macroscopic description the coupling strength involves the same parameter β_2 which appears to be correlated to the effect described above.

Differential cross sections for the first excited state were obtained for the following 30 nuclei: ^{12}C, ^{16,18}O, ^{20,22}Ne, ^{24,26}Mg, ^{28,30}Si, ^{32}S, ^{40}Ar, ^{42,44}Ca, ^{46,48,58}Ti, ^{50,52,54}Cr, ^{54,56,58}Fe, ^{58,60,62,64}Ni, and ^{64,66,68,70}Zn. The cross sections for the different nuclei show sizable differences both in the absolute value and in the shape of the angular distributions.

The absolute values can be parametrized in terms of β_2, the quadrupole deformation parameter obtained as the normalization of a collective form factor deduced from the optical-model potential for the incoming particle. The β_2^{in} values, given in Table I, were obtained from coupled-channel analysis of the above data. These values actually give the deformation of the real central term of the optical potential. The other deformations were modified in order to give a constant $\beta_2 R$ value. The ECIS code by Raynal was used.[34] In this calculation 2^+ states were described as the first excited state of the g.s. rotational or vibrational band. Well depths both for the real and imaginary parts and β_2 values were searched on in a fit to the full angular distribution. Some of the fits produced are shown in Figs. 11 and 13. In comparison to a simple optical-model calculation the quality of the elastic scattering data fit is improved only in the case of strongly deformed nuclei such as ^{20}Ne,

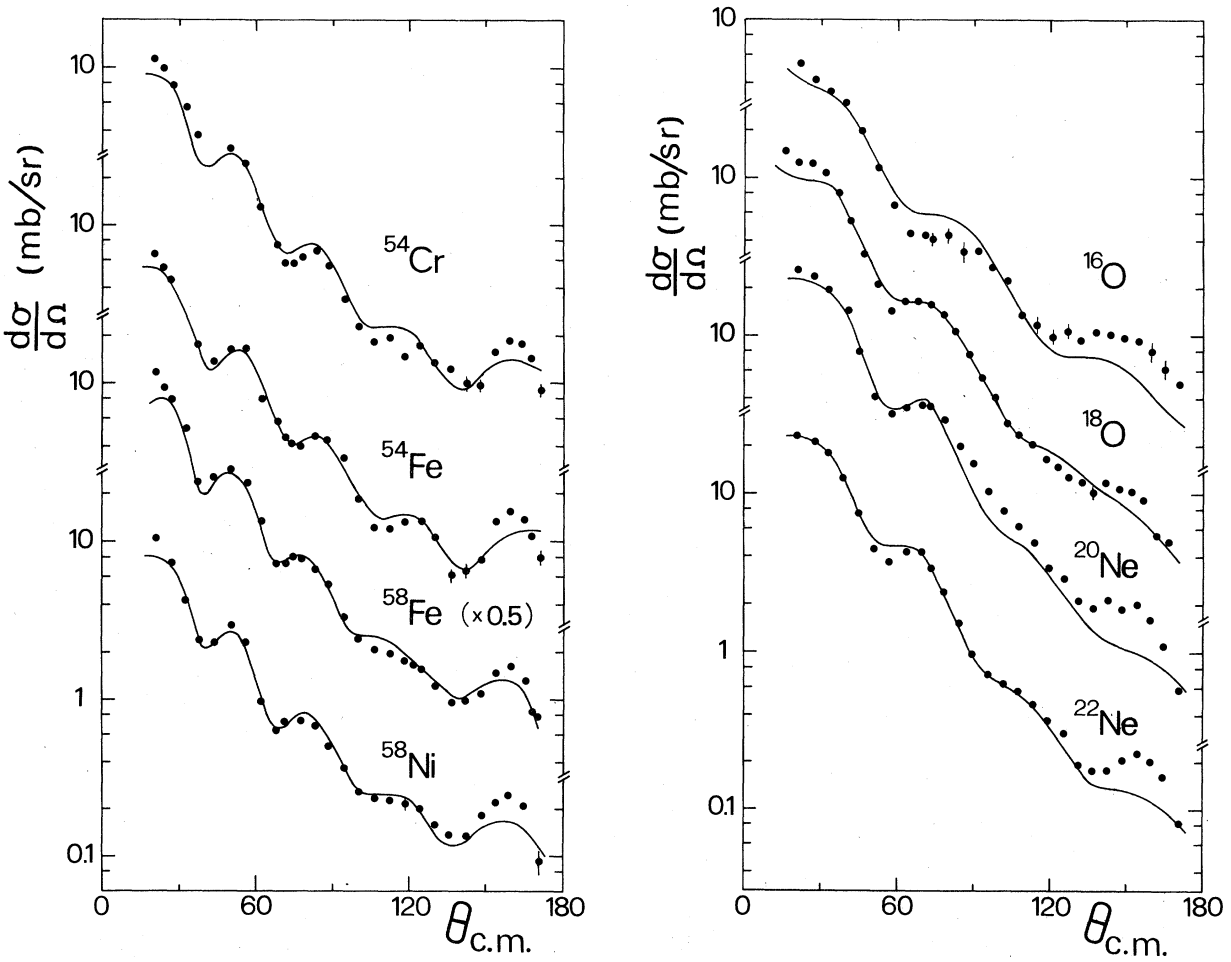

FIG. 13. Inelastic scattering cross sections for the transition to the first 2^+ excited state. The solid lines give the results of the coupled-channel calculations of Fig. 11.

especially at very backward angles. The quality of the fits to the inelastic cross section is generally satisfactory.

Several optical-model potentials and fitting procedures were employed to determine the uncertainty in the β_2 values deriving from the procedure followed in coupled-channels calculations. As resulting from these tests, this uncertainty in β_2^{in} seems confined to a rather small range. This result is not surprising in view of the fact that the calculated cross section is proportional to the square of the volume integrals containing the form factor $\beta_2 RVdf(r)/dr$, where $Vf(r)$ may be approximately identified in the real part of the optical-model potential. If, as in a coupled-channels calculation, the results are also compared with the elastic cross sections and well depths are searched on together with β_2^{in} values, a change in some optical parameter (for example a change in the value of R) is mostly compensated for by adjustment of some other optical-model parameter such as V, so as to leave unvaried the correct value of the volume integral needed by elastic scattering data. The contribution to the uncertainty in β_2^{in} values due to optical-model ambiguities is therefore of a magnitude typical of global quantities, such as the volume integrals, and not of each single parameter. The resulting overall uncertainty in β_2^{in}, also in consideration of systematic and statistical errors in the experimental data, is then of the order of 4%–7%.

In comparing these parameters with those obtained from electromagnetic transitions β_2^{em} it can be recalled that: (1) The two groups of β_2 values are both affected by errors which are on the average of the order of 5%; (2) further contributions to their uncertainty can derive from several approximations which, especially for light nuclei, are rather crude (for instance, the β_2^{em} parameters were deduced[8,10] from electromagnetic transition rates by taking a uniform sharp-edge charge distribution); (3) the two kinds of parameters give, in principle, the deformation of two different physical quantities, the electric charge and the optical-model potential. However, the agreement between the β_2^{em} and β_2^{in} is fairly good. In fact, by averaging over the nuclei studied one obtains $\beta_2^{em}/\beta_2^{in} = 1.09 \pm 0.14$.

It should be observed here that the characteristic behavior, correlated with nuclear deformation, of the volume integrals per nucleon for the imaginary part, found in Sec. IV considering only the elastic scattering, remains substantially the same also in coupled-channels calculations.

As mentioned above, there is some evidence of systematic changes in the shape of the angular distributions which are more evident at backward angles. If one takes the cross section at the backward maximum in the angular distribution σ_{peak} and calculates the ratio $\sigma_{peak}/(R\beta_2)^2$, which corresponds approximately to $\sigma_{back}/\langle\sigma\rangle$, an indication is obtained of the relative yield at backward angles. In Fig. 14 this ratio is plotted against the mass number and compared with σ_{peak} for elastic scattering. The two mass dependences are very similar.

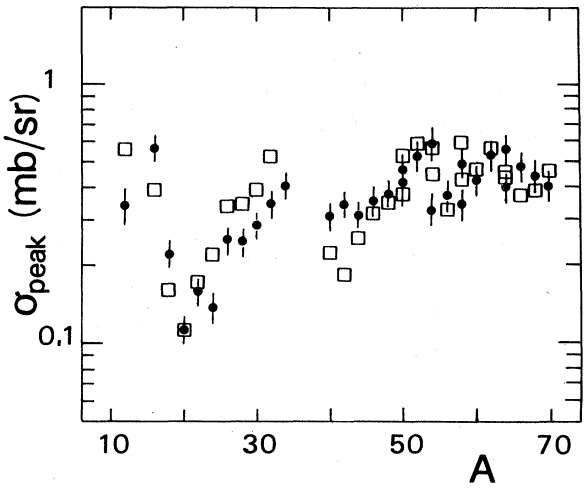

FIG. 14. Peak cross section at the backward maximum in the angular distribution for inelastic scattering to the 2_1^+ state divided by 0.55 $(R\beta_2^{in})^2$ plotted (squares) against mass number. The parameter R is the real well optical-model radius and β_2^{in} is the quadrupole deformation parameter as deduced from the inelastic scattering itself. This ratio is proportional to $\sigma_{back}/\langle\sigma\rangle$. For comparison the dots give the values of σ_{peak} for the elastic scattering cross sections already shown in Figs. 4 and 6. The values given on the vertical scale are obtained when cross sections are measured mb/sr and the radius R in fm.

An enhanced backward yield correlated to nuclear structure therefore seems to also affect inelastic transitions, at least the strong collective transitions to the low-lying 2^+ states.

VI. SUMMARY AND COMMENTS

The systematic measurements reported here and in Paper I provide evidence of nuclear structure effects in proton elastic scattering on light- and medium-weight nuclei. These effects are present also at relatively high incident energies and are in fact observed up to at least 45 MeV proton energy. Their magnitude is largest at the filling of the $1p$ shell. In the energy range 30–35 MeV the cross section at backward angles for proton elastic scattering on ^{14,15}N and ^{16,17}O is larger by about one order of magnitude than that for beryllium or neon isotopes. In this mass region, shell effects are also present in the forward angle cross section,

which is enhanced by about 15%. This enhancement corresponds to a decrement in the total reaction cross section.

Similar features in the data were also observed at the filling of the $2s$-$1d$ shells. In this region, however, the magnitude of the backward effect is smaller and produces an increase in the cross section value at backward angles limited to a factor of about two with respect to the value for deformed nuclei. No evidence of the forward effect has been found in this mass region.

Detailed analysis of all the experimental data provides strong evidence that these effects are correlated to the collective properties of the nuclei involved. The systematic study of proton scattering at 35.2 MeV shows, in fact, a definite correlation between the mass dependence of the yield in the elastic channel and the quadrupole deformation parameters β_2. The elastic yield is maximum for spherical and minimum for deformed nuclei. The correlation between cross sections and deformation parameters is ultimately the same for all nuclei, namely for even-even and odd-A nuclei, if one uses the β_2 values as derived by considering the coupling strength affecting the dynamics of the scattering process rather than the static geometrical deformations. An enhancement in the relative yield at backward angles, with the same nuclear structure dependence, was also found for the inelastic scattering leading to the first 2^+ state in even-even nuclei.

Further clues are provided by the magnitude of the above effects and by their energy dependence. It is difficult to ascertain whether the effect found in the forward part of the differential cross sections is also present at relatively low energies due to the large contributions from compound nucleus resonances and from the opening of reaction channels. It is however certainly present at energies as low as 20 MeV. A possible explantion could be related to the smaller number of open channels for nuclei near ^{16}O leading to a lower total reaction cross section and consequently to a larger elastic cross section. This explanation cannot be valid for the backward effect both because of its magnitude and its energy dependence. It has been shown in fact that the effect at backward angles becomes very evident only above 26 MeV and reaches its maximum only in the energy region between 30 and 40 MeV.

An enhancement at backward angles has also been found in the elastic scattering of other light projectiles. The most widely known is the anomalous large angle scattering (ALAS) for alpha particles. However some features of the data reported here, like the presence of effects also at forward angles and the correlation with collective properties, seem typical of proton scattering.

An optical-model calculation satisfactorily reproduces the cross sections at forward angles, when average potentials with a smooth mass and energy dependence are used. This is not true of cross sections at backward angles for spherical nuclei above 26 MeV, where the proton elastic scattering may be considered anomalous in comparison to a conventional optical-model calculation. It was shown in Paper I that the use of nonstandard radial distributions of the potentials, as suggested by recent folding-model calculations and by some successful attempts in fitting ALAS data, can lead to some improvements but fails to solve the main difficulty found in these optical-model calculations, that is, it fails to reproduce the energy dependence of the angular position of the backward maximum. As pointed out, in spite of the rather large number of parameters used, this result is similar to that found by Brieva in the comparison between folding-model calculations and experimental data for ^{40}Ca above 26 MeV.

In our opinion it is still an open question whether the folding model or more generally the optical-model even including a more detailed description of the nuclear structure, will adequately describe the mass dependence of proton scattering in the energy region here studied. Our results indicate that a dependence from the deformation parameters β_2 of the imaginary part of the optical-model potential can reproduce the nuclear structure effects at forward but not at backward angles.

An alternative approach, adopted by some authors,[35-37] is to evaluate explicitly the contributions to the optical potentials due to the coupling with certain classes of reaction channels. The most important "doorways" for the absorption of protons are expected to be direct inelastic scattering and direct rearrangements. Recently the couplings with high-lying inelastic channels and with the (p,d) reaction have been considered.[35,36] Both couplings give an enhancement in the elastic yield, which results in a backward maximum in the angular distribution. This enhancement is larger at an energy of about 10 MeV for the intermediate particle if the process is described as a two-step (p,p',p) or (p,d,p). If one considers the energy position of giant resonances, which act as a clustering of possible intermediate states for the (p,p',p) process, as well as the values of the (p,d) thresholds, it becomes clear why the backward effect is maximum between 30 and 40 MeV. This result is also confirmed by some preliminary two-step calculations we have performed for a wide range of nuclei and incident energies.

The A dependence is less straightforward. In fact the differences found between elastic cross

sections for magic and collective nuclei cannot be explained on the basis of simple considerations on deuteron thresholds, single particle energies or the energy distribution of the quadrupole strength. More explicitly, the excitation of the intermediate states should be fairly similar for magic and collective nuclei.

The structure of the nuclei involved might however determine the depletion process of these states and consequently their effect on the elastic channel. A complete calculation should therefore utilize detailed knowledge of spectroscopic factors for transitions between excited states.

For the time being it can only be observed that in spite of some success in fitting specific data, the present theoretical interpretations leave open the problem of explaining in detail the phenomenology of proton scattering. This phenomenology, on the other hand, has attained a satisfactory degree of accuracy; its main features are now better known and should allow exhaustive tests of theoretical models.

[1]E. Fabrici, S. Micheletti, M. Pignanelli, F. G. Resmini, R. De Leo, G. D'Erasmo, A. Pantaleo, J. L. Escudié, and A. Tarrats, Phys. Rev. C 21, 830 (1980).

[2]C. C. Kim, S. M. Bunch, D. W. Devins, and H. H. Forster, Nucl. Phys. 58, 32 (1964); B. W. Ridley and J. F. Turner, *ibid.* 58, 497 (1964); O. Karban, J. Lowe, P. D. Greaves, and V. Hnizdo *ibid.* A133, 255 (1969); H. S. Sandhu, *ibid.* A146, 163 (1970); P. D. Greaves, V. Hnizdo, J. Lowe, and O. Karban, *ibid.* A179, 1 (1972); D. G. Montague, R. K. Cole, P. S. Lewis, C. N. Waddell, and D. L. Hendrie, *ibid.* A199, 433 (1973); R. De Swiniarski, A. Genoux-Lubain, G. Bagieau, J. F. Cavaignac, D. H. Worledge, and J. Raynal, Phys. Lett. 43B, 27 (1973); R. De Swiniarski, F. G. Resmini, C. Glashausser, and A. D. Bacher, Helv. Phys. Acta 49, 227 (1976).

[3]R. De Leo, G. D'Erasmo, E. Fabrici, S. Micheletti, A. Pantaleo, M. Pignanelli, and F. G. Resmini, Report No. INFN/BE-78/8, Frascati, 1978.

[4]L. H. Johnston, D. H. Service, and D. A. Swenson, IRE Trans. Nucl. Sci. 5, 95 (1958).

[5]R. S. Mackintosh and L. A. Cordero, Phys. Lett. 68B, 213 (1977).

[6]A. Tarrats and J. L. Escudié, in *Microscopic Optical Potentials*, *Lecture Notes in Physics*, edited by H. V. V. Geramb (Springer, New York, 1979), Vol. 89, p. 200.

[7]P. M. Endt and C. Van Der Leun, Nucl. Phys. A235, 27 (1974).

[8]P. H. Stelson and L. Grodzins, Nucl. Data 1, 21 (1965).

[9]P. M. Endt and C. Van Der Leun, Atomic Data and Nucl. Data Tables 13, 67 (1974).

[10]S. Raman, W. T. Milner, C. W. Nestor Jr., and P. H. Stelson, in *Proceedings of the International Conference on Nuclear Structure, Tokyo, 1977,* edited by T. Marumori (Physical Society of Japan, Tokyo, 1978), p. 79, and private communication.

[11]E. T. Baker, S. Davis, C. Glashausser, and A. B. Robbins, Nucl. Phys. A250, 79 (1975).

[12]G. H. Fuller and V. W. Cohen, Nucl. Data Tables A5, 433 (1969).

[13]G. T. A. Squier, E. A. McClatchie, A. R. Johnston, R. J. Batten, J. B. A. England, and F. G. Kingston, Nucl. Phys. A119, 369 (1968).

[14]J. F. Cavaignac, S. Jang, and D. H. Worledge, Nucl. Phys. A243, 349 (1975).

[15]B. G. Harvey, J. R. Meriwether, J. Mahoney, A. Bussière de Nercy, and D. J. Horen, Phys. Rev. 146, 712 (1966).

[16]W. Scholz and F. B. Malik, Phys. Rev. 153, 1071 (1967).

[17]M. Nakamura, in *Proceedings of the International Conference on Nuclear Structure, Tokyo, 1977* [J. Phys. Soc. Jap. 44, Suppl. 577 (1978)].

[18]R. H. Knight, W. Scholz, and F. B. Malik, in *Proceedings of the EPS International Conference on the Physics of Medium-light Nuclei, Florence, 1977,* edited by P. Blasi and R. A. Ricci (Editrice Compositori, Bologna, 1977), p. 158.

[19]J. R. Confort, P. Wasielewski, F. B. Malik, and W. Scholz, Nucl. Phys. A160, 385 (1971).

[20]W. G. Love and F. T. Baker, Phys. Lett. 35, 1219 (1975).

[21]D. L. Pham and R. De Swiniarski, Nuovo Cimento 41A, 543 (1977).

[22]F. D. Becchetti and G. W. Greenlees, Phys. Rev. 182, 1190 (1969).

[23]W. D. Myers, Nucl. Phys. A204, 465 (1973).

[24]J. P. Jeukenne, A. Lejeune, and C. Mahaux, Phys. Rev. C 16, 80 (1977).

[25]J. W. Negele, Phys. Rev. C 1, 1260 (1970).

[26]H. V. v. Geramb, F. A. Brieva, and J. R. Rook, in *Microscopic Optical Potentials, Lecture Notes in Physics*, edited by H. V. V. Geramb (Springer, New York, 1979), Vol. 89, p. 104.

[27]W. F. McGill, R. F. Carlson, T. H. Short, J. M. Cameron, J. R. Richardson, I. Šlaus, W. T. H. van Oers, J. W. Verba, D. J. Margaziotis, and P. Doherty, Phys. Rev. C 10, 2237 (1974).

[28]I. Šlaus, D. J. Margaziotis, R. F. Carlson, W. T. H. van Oers, J. R. Richardson, Phys. Rev. C 12, 1093 (1975).

[29]R. F. Carlson, A. J. Cox, J. R. Nimmo, N. E. Davison, S. A. Elbakr, J. L. Horton, A. Houdayer, A. M. Sourkes, W. T. H. van Oers, and D. J. Margaziotis, Phys. Rev. C 12, 1167 (1975).

[30]T. N. Nasr, A. M. Sourkes, D. J. Margaziotis, R. F. Carlson, and A. J. Cox, Can. J. Phys. 56, 56 (1978).

[31]D. G. Montague, R. K. Cole, M. Makino, and C. N. Waddell, Nucl. Phys. A199, 457 (1973).

[32]H. F. Lutz, D. W. Heikkinen, and W. Bartolini, Nucl. Phys. A198, 257 (1972).

[33]W. T. H. van Oers and J. M. Cameron, Phys. Rev. 184, 1061 (1969).

[34]J. Raynal, CEN-Saclay Report No. D. Ph/tN° 71/7,

Code ECIS, 1971.
[35]C. L. Rao, M. Reeves III, and G. R. Satchler, Nucl. Phys. A207, 182 (1973); P. W. Coulter, and G. R. Satchler, *ibid.* A293, 269 (1977).
[36]R. S. Mackintosh and A. M. Kobos, Phys. Lett. 62B, 127 (1977); J. Phys. G 5, 359 (1979).
[37]N. Vinh Mau and A. Bouyssy, Nucl. Phys. A257, 189 (1976).